JOURNAL OF MATERIALS SCIENCE 33 (1998) 1263–1271

# A TEM investigation of $M_{23}C_6$ carbide precipitation behaviour on varying grain boundary misorientations in 304 stainless steels

E. A. TRILLO, L. E. MURR
*Department of Metallurgical and Materials Engineering, The University of Texas at El Paso, TX 79968 USA*

Transmission electron microscopy (TEM) along with electrochemical potentiokinetic reactivation (EPR) testing was performed on different grades of 304 stainless steel (0.01, 0.025, 0.05, and 0.07% C) in order to assess the sensitization and precipitation behaviour on different grain boundary misorientations. The materials were heat treated at 670 °C for 50 h to subject the materials to the sensitization regime. The EPR data and TEM observations revealed that when the amount of carbon was increased the degree of sensitization increased along with the density of precipitates. Large angle misorientations ($\Theta > 15^\circ$) were prevalent in all the carbon content materials and the $\{1\,1\,0\}$ grain surface orientation was found to be the major texturing orientation. The steels with lower carbon contents nucleated a few small precipitates on high angle grain boundaries, while larger amounts of carbides were observed on lower angle grain boundaries for the higher carbon contents. It was deemed that higher carbon contents required lower energies to nucleate and grow precipitates. A carbon content threshold was found (above 0.05% C) in which precipitates fully saturate the grain boundary. Precipitation followed the energies of different types of boundaries. The highest energy boundary (general random grain boundary) nucleated precipitates first, then precipitation followed on non-coherent twin boundaries, and was not observed on coherent twin boundaries. A ''critical nucleation energy'', $\gamma_{gb(crit.)}$, was therefore found to exist at which precipitation will occur on a boundary. This value was found to be in the range of $16\ mJ\ m^{-2} < \gamma_{gb(crit.)} < 265\ mJ\ m^{-2}$ which corresponds to the energies of special boundaries (coherent and non-coherent portions of twins respectively) at the ageing temperature of 670 °C. © *1998 Chapman & Hall*

## 1. Introduction

Since the early observations of Stickler and Vinckier [1] on commercial grades of austenitic (Fe–Ni–Cr) stainless steels it has been known that sensitization and $M_{23}C_6$ carbide precipitation will occur first on the highest energy interfaces (random grain boundaries), then on recognizable special (lower-energy) boundaries such as non-coherent twin interfaces. In earlier work [1–6], and in some recent studies, it has been shown that low $\Sigma$ boundaries (like coherent twin boundaries) resist corrosion. Sensitization and precipitation will thus occur last on these coherent twin boundaries. However, more recent work by Advani *et al.* [7] has provided some transmission electron microscopy (TEM) evidence which suggests that carbides do not actually nucleate and grow on $\Sigma 3$ (coherent twin) boundaries, but nucleate and grow on higher-energy, non-coherent steps (including microsteps) on these boundaries and then, in some specific crystallographic instances, they grow parallel to the coherent twin boundary, coincident with a specific $\{1\,1\,1\}$ plane [8].

If there is no sensitization and precipitation on coherent twin boundaries ($\Sigma 3$), and if ideally the occurrence of these boundaries could be selectively increased over all other interfaces in a polycrystalline, stainless alloy, the overall, bulk sensitization would be reduced, and the material would become more corrosion resistant. This concept has been discussed by Watanabe [6, 9] and others [7, 10], not only for enhanced corrosion resistance, but for mechanical and other properties as well. Watanabe [9] has referred to this strategy of interfacial manipulation as "grain boundary design and control". Such control has been difficult to achieve. Palumbo *et al.* [11] have also addressed the role of annealing twin formation on the basis of both energetic and geometric considerations, and demonstrated that a microstructure consisting entirely of low-$\Sigma$ CSL boundaries, which they called a "twin limited microstructure", could be attained in principle by annealing twin formation. In recent work reported by Trillo *et al.* [12], the number of twins per grain in 304 stainless steel did not change from a value of 2 per grain for a variety of thermomechanical

0022–2461  

processes, which produced grain sizes ranging from around 15 μm to 150 μm. However, recent work reported by Lin *et al.* [13] has described a proprietary thermomechanical process for a commercial grade Alloy 600 (a Ni–Fe–Cr stainless alloy with 0.06% (wt) C) where the special grain boundary ($\Sigma \leqslant 29$) frequency was increased from 37 to 71%. A corresponding decrease in the bulk intergranular corrosion susceptibility in both the solution annealed and sensitized condition was also obtained. In related work, Mizera *et al.* [14] have also recently demonstrated that changes in texture increase the number of special (CSL) grain boundaries, or more generally alter the "character" of the grain boundaries in a 316 stainless steel.

While techniques involving orientation imaging microscopy [15] and other, related automated techniques for rapidly determining texture (pole figures), or electron backscattered diffraction in the scanning electron microscope (SEM) [16–18], can provide for quantitative evaluations of crystallographic misorientation data, they cannot simultaneously image either specific grain boundaries, or precipitates associated with these boundaries. As a consequence, there is neither quantitative nor qualitative information relating grain boundary misorientations to specific sensitization issues such as the actual confirmation that carbides did in fact precipitate in grain boundaries of known misorientations.

Both sensitization and precipitation are affected by interfacial energy. That is, as the energy is reduced (as implicit in reductions of $\Sigma$ values) there is a concomitant reduction in sensitization and precipitation. Consequently, as the boundary misorientation changes, there should be some recognizable variation in either the frequency or size of precipitates. In a paper by Aaronson *et al.* [19] the concept of heterogeneous nucleation at an $\alpha$:$\alpha$ grain boundary was discussed. His work, however, does not emphasize the importance of the interfacial energy of the grain boundary itself, instead it correlates the interfacial energies of the coherent faces of the growing precipitate to the Helmholtz free energy. Because there have been no systematic attempts to elucidate the role of interfacial energy and misorientation, on sensitization and precipitation, it was the objective of this study to provide, for the first time, some preliminary observations of carbide precipitation not only as a function of grain boundary misorientation, but also as a function of carbon content.

## 2. Experimental procedures

The four stainless steels utilized in this study were received in plate form (6.25 mm in thickness) and contained the chemical compositions listed in Table I. The main difference between them is the increase in carbon content (0.01% to 0.07% C). The mill-processed plate was sectioned into $6.25 \times 6.25$ mm samples and heat treated at 670 °C for 0.1 to 500 h. The samples were then polished down to a 1 μm diamond finish in preparation for an electrochemical potentiokinetic reactivation (EPR) test. This test determines the degree of sensitization (DOS) in a material.

TABLE I Chemical composition in (wt %)

| C | Cr | Ni | Mo | N | P | Fe | Grain size (μm) |
|---|---|---|---|---|---|---|---|
| 0.011 | 18.13 | 8.92 | 0.34 | 0.08 | 0.022 | balance | 50 |
| 0.025 | 18.35 | 9.08 | 0.37 | 0.08 | 0.026 | balance | 40 |
| 0.05 | 18.31 | 8.08 | 0.35 | 0.084 | 0.031 | balance | 35 |
| 0.07 | 18.23 | 8.15 | 0.35 | 0.08 | 0.035 | balance | 40 |

After EPR testing, transmission electron microscopy was performed on the four different carbon contents aged for 50 h at 670 °C. The actual electron microscope protocols consisted in identifying grain boundaries where the selected-area diffraction pattern could be clearly identified as [1 1 0] on either side of the interface. This orientation was chosen because of the prominent $\langle 1\,1\,0 \rangle$ texturing in the test specimens, and the fact that this orientation contains a unique direction $[1\,\bar{1}\,0]$.

It is well known that random grain boundaries possess 5 degrees of freedom [20]. Thus, by demanding that the neighbour grains, establishing a particular grain interface, have the same [1 1 0] surface orientation in the TEM thin section, provides an unquestionable measurement of the misorientation. This measurement is related as a simple rotation about this crystallographic zone axis in the context of the grain boundary plane trace. It was not in the interest of this study to establish the crystallographic coincidence for the grain interface, only the misorientation angle for the same [1 1 0] neighbouring crystals. It will be assumed, therefore, that the relative grain boundary free energy is generally related to this simple misorientation angle measurement. $E_{gb} = \gamma_{gb} \infty \Theta$ [20], where $E_{gb}$ is the grain boundary free energy, $\gamma_{gb}$ is the grain boundary interfacial energy. Each different material had at least eight to nine grain boundary observations. While this is a statistically small sample, it did allow trends to be established, especially through comparative histograms representing the data.

In addition to the recording of specific grain boundary (bright-field) images and the associated, neighbouring SAD patterns, the precipitate density was also measured. The precipitate density was measured as the number of precipitates per unit area of grain boundary ($n/A$, where $A = 0.5\ \mu m^2$) as a fiducial area. These measurements required the determination of accurate foil thickness in the grain boundary area of interest, and of specific grain boundary geometries [16].

## 3. Results and discussion

### 3.1. EPR-degree of sensitization

The results of the EPR tests for the four carbon contents are reproduced in Fig. 1. The *x*-axis is the heat treatment time at 670 °C and the *y*-axis is the EPR-DOS or the degree of sensitization in a material. A steel with a given carbon content (except the

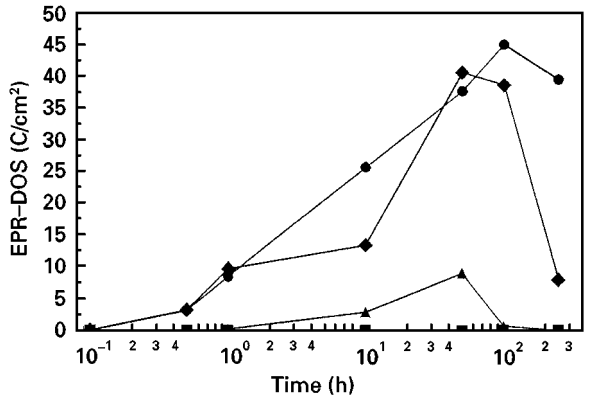


*Figure 1* EPR-DOS versus heat treatment time for the four carbon contents at 670 °C. Larger carbon contents display an increase in the degree of sensitization (DOS). (■) 0.01% C; (▲) 0.025% C; (●) 0.05% C; (◆) 0.07% C.

0.01% C) will display an increase in the degree of sensitization, peak at a certain DOS value, and then decrease in DOS (known as desensitization or healing). The 0.01% C material, however, does not show any significant sensitization occurring at this temperature. In addition, the graph clearly demonstrates a general increase in EPR-DOS with increasing carbon content at any given ageing time. At 50 h ageing time, the 0.05% C material is slightly higher in DOS than the 0.07% C material. Above about 0.05% C the sensitization may not be influenced in a simple linear fashion.

Chromium carbide precipitation in 304 stainless steels is governed by the thermodynamics of carbon concentration and the kinetics of chromium diffusion [21]. The EPR-DOS data clearly demonstrate the effect of carbon content. The 0.01% C material did not sensitize because the material does not have enough carbon in the system to produce significant amounts of carbides that would result in the depletion of chromium at the grain boundaries.

## 3.2. Carbide density measurements

The amount of precipitation per unit length of grain boundary was measured on all observed misorientations for the four carbon contents (0.01, 0.025, 0.05, 0.07% C) for 50 h ageing at 670 °C. The results of that analysis are seen in Fig. 2. For the lowest carbon content of 0.01% C there were a small number of small carbides on one highly misoriented grain boundary ($\Theta = 67^\circ$), Fig. 2a. The 0.025 and 0.05% C materials (Fig. 2b and c) display increasing carbide density and size that occur on relatively highly misoriented grains ($31^\circ < \Theta < 85.6^\circ$). In contrast, the 0.07% C material shows a dense precipitate growth which extends to lower misorientations ($17^\circ < \Theta < 68^\circ$).

The effect of carbon content and grain boundary misorientations on carbide precipitation can be seen through selected, typical transmission electron micrographs in Figs 3 to 6. Microscopic observations in the 0.01% C material are shown in Fig. 3a and b. Fig. 3 also illustrates the general procedures utilized in measuring the grain boundary misorientation angles of Fig. 2. The lowest angle grain boundary ($\Theta = 10^\circ$) contains no observable precipitates, while the high-angle grain boundary ($\Theta = 67^\circ$) reveals very fine precipitates. In fact, taking into account all the samples that were observed for this study (including those not reported), precipitates were found on only one grain boundary in the 0.01% C material. The 0.025% C material also did not have any carbides at a very low grain boundary misorientation ($\Theta \cong 2^\circ$, in Fig. 4a), but did have carbides growing at a larger misorientation ($\Theta = 65^\circ$ in Fig. 4b), similar to the observations for the 0.01% C material in Fig. 3. The higher carbon contents ($\geqslant 0.05\%$ C) on the other hand, displayed carbides on grain boundaries on the smallest misorientations observed as well as the large misorientations, as shown in Fig. 5a and b and Fig. 6a and b for 0.05% C and 0.07% C, respectively. The 0.07% C shows the increase in carbide density that was previously documented quantitatively in Fig. 2.

It was also noted that carbides were present on all grain boundaries in the 0.05% and 0.07% C materials, including those not reported here. In addition, the carbides are more closely spaced in the 0.07% C material than the 0.05% C material.

The carbide density data (Fig. 2) and the TEM micrographs (Figs 3 to 6) both demonstrate the necessity of the grain boundary to provide a requisite energy to nucleate (heterogeneously) and grow carbides. Grain boundary misorientations represent a change in energy in this system, because increasing the grain boundary misorientation increases the interfacial free energy of the boundary [20]. To nucleate a precipitate in the 0.01% C system, a correspondingly large energy was required, and implicitly a large misorientation was necessary ($\Theta = 67^\circ$). The largest carbon content (0.07% C) did not require large grain boundary misorientations (and corresponding energies) to nucleate and grow precipitates as seen in the density data (Fig. 2d) and the TEM micrographs (Fig. 6a and b). This trend suggests that higher carbon contents require somewhat lower energies to nucleate and grow precipitates as a consequence of the altered thermodynamics due to a preponderance of carbon.

## 3.3. Grain boundary misorientation distribution

Fig. 7 is a set of five graphs that show the measured grain boundary misorientation distributions for the four different carbon contents (Fig. 7a to d) and, for the combination of all carbon contents (Fig. 7e). The two lowest carbon contents (0.01% and 0.025% C) in Fig. 7a and b show that several grain boundaries did not contain precipitates. The higher carbon contents (0.05% and 0.07% C), however, display carbide formation on all observed grain boundaries. One should also note that although the 0.01% and 0.025% C materials contained some low-angle grain boundary misorientations ($\Theta < 15^\circ$), the tendency for large-angle misorientations were prevalent, as seen when all

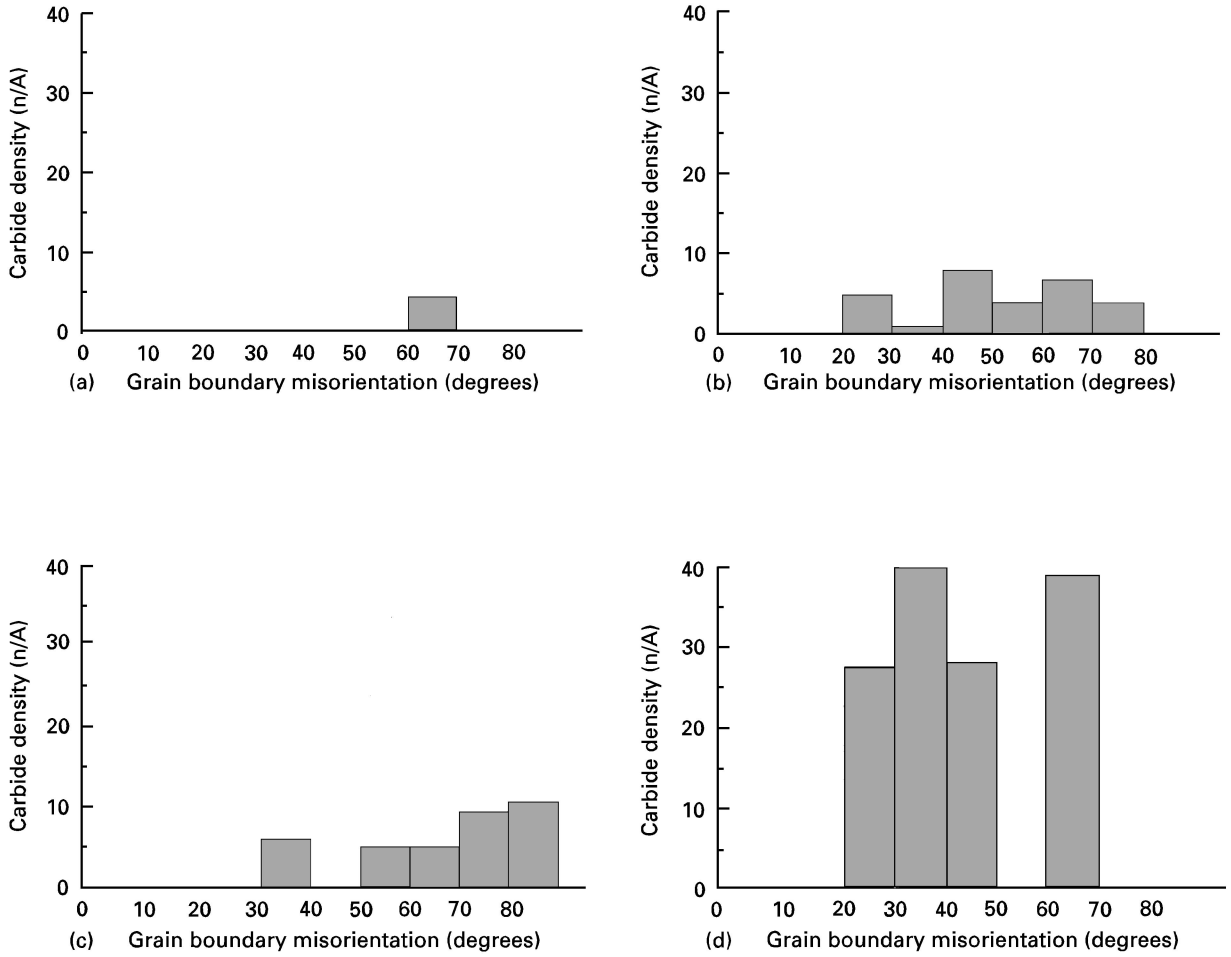


*Figure 2* Carbide density measurements per unit length of the grain boundary at varying misorientations in the (a) 0.01% C, (b) 0.025% C, (c) 0.05% C and (d) 0.07% C materials. Generally, lower carbon contents precipitate carbides on higher grain boundary misorientations, while higher carbon contents precipitate carbides on much lower grain boundary misorientations.

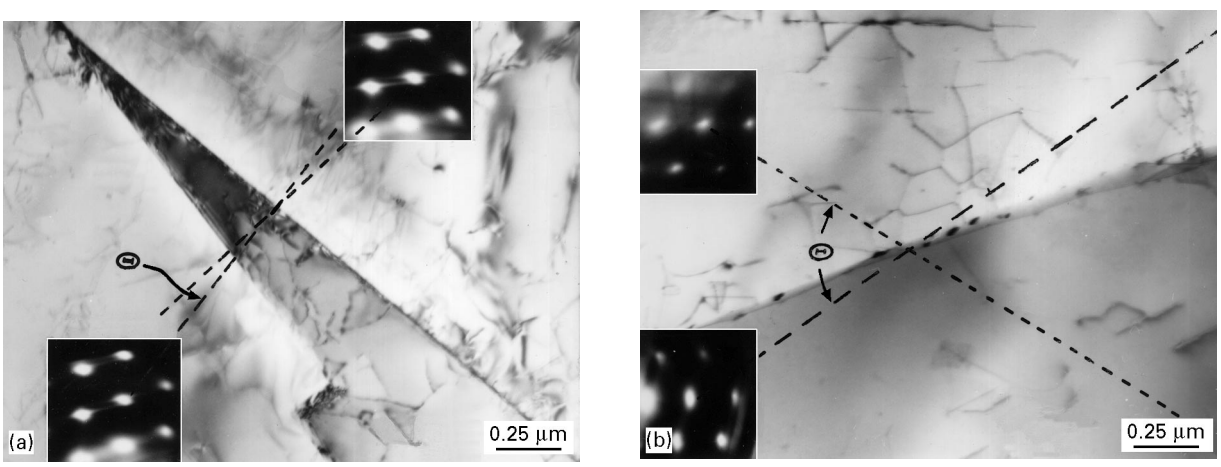


*Figure 3* TEM micrographs of the 0.01% C material at 670 °C at 50 h heat treatment time. (a) grain boundary misorientation of 10° and (b) grain boundary misorientation of 67°. Note associated [1 1 0] SAD patterns corresponding to each neighbour grain are inserted in the proper image coincidence. The corresponding [1 1 0] directions are shown dotted as extensions from the pattern. The grain boundary misorientation angle, Θ, is measured as the angle between these directions as shown.

observations were combined in the summary histogram of Fig. 7e.

## 3.4. Carbide precipitation at twin boundaries

Along with observations on general (random) grain boundaries, we investigated the $M_{23}C_6$ carbide precipitation behaviour on annealing twins as well. One of the reasons for these observations was that the coherent twin boundaries provide a specific and energetically unique reference interface with an interfacial free energy (20 mJ m$^{-2}$) that is known at the same temperature (1060 °C) as the average high-angle (random) grain boundary free energy. It also represents the smallest ΣCSL boundary (Σ3). Non-coherent

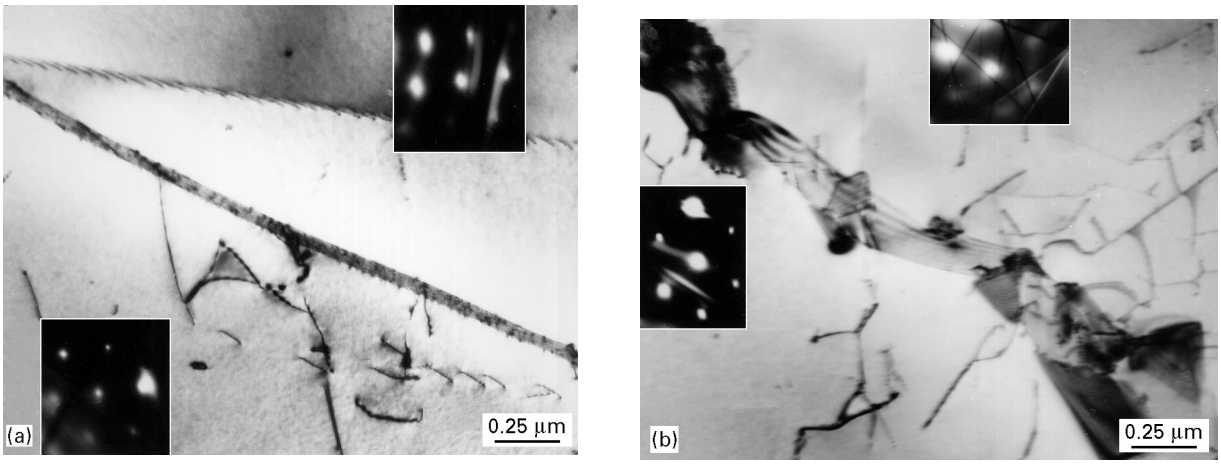


*Figure 4* TEM micrographs of the 0.025% C material at 670 °C at 50 h heat treatment time for (a) $\Theta = 2^\circ$ and (b) $\Theta = 65^\circ$. Precipitates are only visible on the highest grain boundary misorientation in (b).

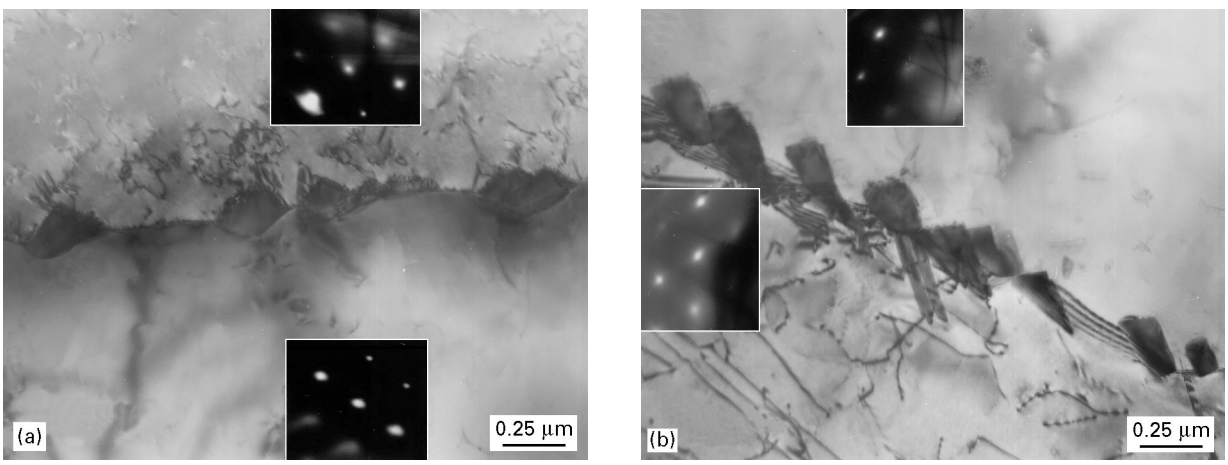


*Figure 5* TEM micrographs of the 0.05% C material at 670 °C and at 50 h heat treatment time for (a) $\Theta = 31^\circ$ and (b) $\Theta = 85.6^\circ$. Precipitates are found on both high and low grain boundary misorientations.

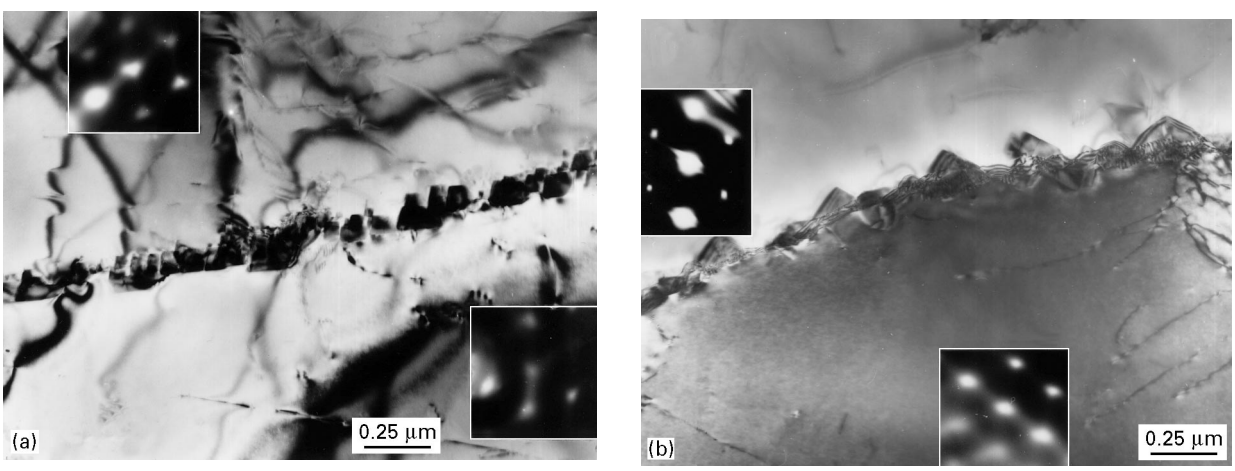


*Figure 6* TEM micrographs of the 0.07% C material at 670 °C and at 50 h heat treatment time for (a) $\Theta = 17^\circ$ and (b) $\Theta = 68^\circ$. Both grain boundary misorientations display a dense precipitate structure.

steps on annealing twins also represent a set of special boundaries in the stainless steel system in which the exact misorientation is not known but the average interfacial free energy has also been determined at the same reference temperature as the coherent twin boundary free energy [20]. Figs 8 and 9 document the typical precipitation behaviour that was observed on twins in 304 stainless steel at the experimental temperature and time. Many of the observed twins were in close or immediate proximity to typical, random grain boundaries. The coherent portions of the twins show no carbide precipitation while the grain boundaries have nucleated and grown carbides, Fig. 8a and b. Fig. 9a relates the non-coherent twin behaviour to grain

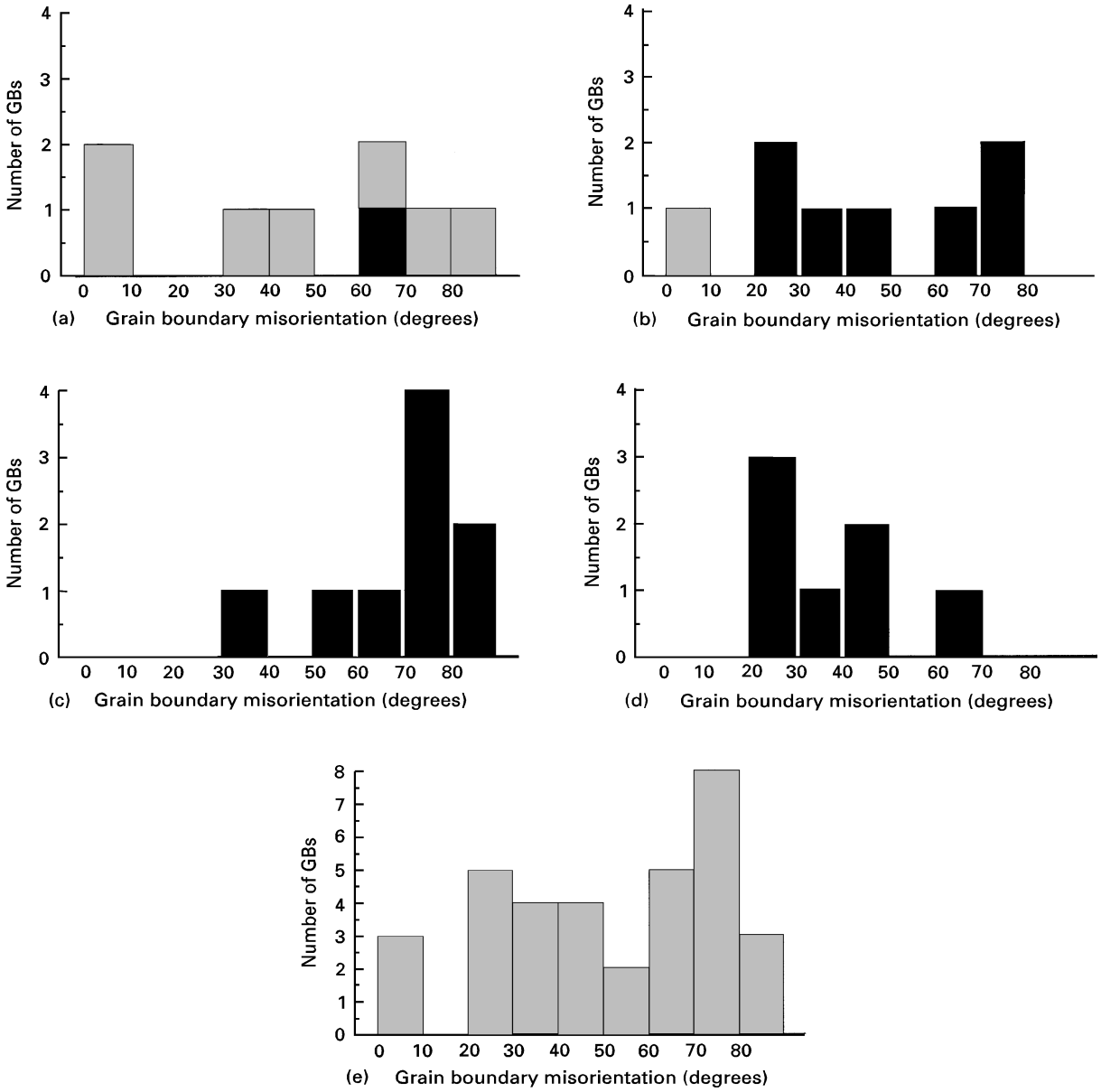


*Figure 7* Grain boundary misorientation distribution that shows the number of boundaries observed (□) and those boundaries that contained carbides (■) for the (a) 0.01% C, (b) 0.025% C, (c) 0.05% C, (d) 0.07% C and (e) all carbon contents combined. There was a tendency toward larger grain boundary misorientations ($\Theta > 15°$) in this material.

boundary effects. Precipitation will occur on the grain boundary itself and on the non-coherent portion of the twin; however, precipitates are absent on the coherent portion. Fig. 9b also displays carbides growing exclusively on the non-coherent portion of the twin.

The effect of increasing carbon content can be seen in Fig. 10a–d. Here, the coherent and non-coherent portions of annealing twins (including steps and twin ends) are seen for each of the four carbon contents. Precipitation did not occur on any twin-related interfaces in the 0.01% C material. However, at 0.025% C and above the density of precipitates increases on the non-coherent portions of the twins. Again, no precipitation behaviour was observed on the coherent portions of the twins. In Fig. 10d a few precipitates seem to be growing on the lower portion of the coherent twin boundary; however, when magnified, the carbides will show that they are growing on a micro-non-coherent or micro-step type boundary.

The physical evidence for carbide precipitation on annealing twin interfaces is concurrent with the observations reported for increasing grain boundary misorientation cases in Fig. 7. This is because of the differing energetic sites that twins provide in contrast to random grain boundaries. The measured, average grain boundary free energy for 304 stainless steel is $835\ \mathrm{mJ\,m^{-2}}$ at 1060 °C [20, 25]. The corresponding temperature coefficient of interfacial free energy was found to be $\mathrm{d}\gamma_{gb}/\mathrm{d}T = -0.49\ \mathrm{mJ\,m^{-2}\,°C^{-1}}$ [20]. The average grain boundary free energy at the experimental ageing temperature of 670 °C in this research is then estimated as $1026\ \mathrm{mJ\,m^{-2}}$. Although the average value of the non-coherent twin boundary free energy has not been experimentally measured directly, the ratio $\gamma_{TB}/\gamma_{gb}$ was experimentally measured to be 0.25 at 1060 °C [25]. If it is assumed that this ratio will remain constant down to the 670 °C ageing temperature, then the corresponding value of $\gamma_{TB}$ is $265\ \mathrm{mJ\,m^{-2}}$. Finally, the measured coherent twin

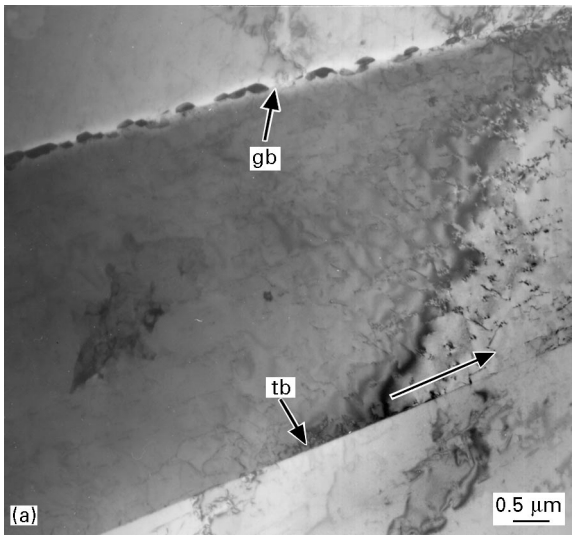


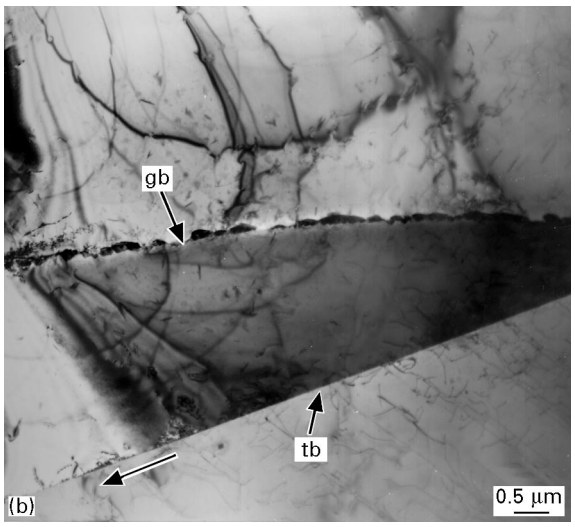


*Figure 8* TEM micrographs of precipitation behaviour on grain boundaries (gb) compared with coherent twin boundaries (tb) forming adjacent to the grain boundary. Samples are of the 0.07% C material at a heat treatment of 50 h at 670 °C. (a) and (b) show similar situations where the coherent twin boundary is coincident with the (1 1 1) plane in the [1 1 2] direction shown by the arrow.

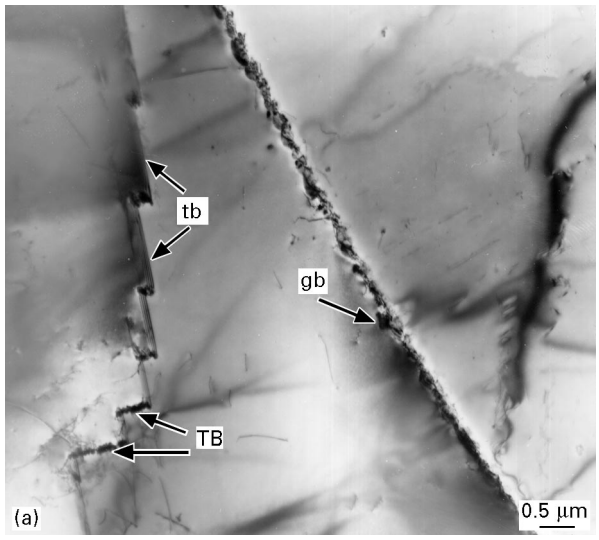


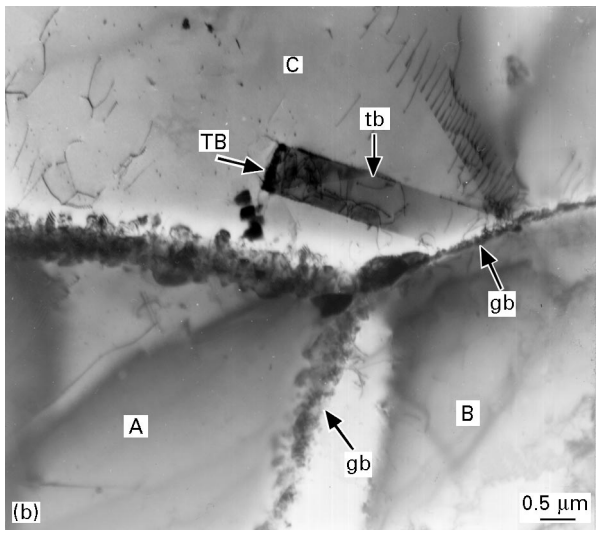


*Figure 9* TEM micrographs of precipitation on grain boundaries (gb) versus the non-coherent twin boundaries and steps (TB) and coherent twin boundaries (tb) in 304 stainless steel. Samples are from the 0.07% C material heat treated for 50 h at 670 °C. (a) non-coherent steps (TB) along coherent twin boundaries (tb), (b) grain boundary triple point for grains A, B, and C. Grain C shows an annealing twin with precipitates on the non-coherent twin end (TB).

boundary free energy is 19 mJ m$^{-2}$ at 1060 °C; the temperature coefficient, $d\gamma_{tb}/dT = +0.007$ [25]. Consequently, the average coherent twin boundary free energy at 670 °C is estimated to be 16 mJ m$^{-2}$. The energies adjusted to the experimental ageing temperature of 670 °C became $\gamma_{gb}:\gamma_{TB}:\gamma_{tb} = 1026:265:16$ mJ m$^{-2}$. The non-coherent steps have nominal energies about four times less than random high-angle boundaries over a wide temperature range and the coherent twin boundaries possess an interfacial free energy that is roughly a factor 40 below that of random high-angle boundaries. This energy difference has a definite effect on precipitation behaviour. Carbides can readily be seen at grain boundaries and on the non-coherent portions of the twins (high energy sites) in Fig. 10b–d and Fig. 9a and b, but are not at all seen on the coherent portions (lowest energy sites) in any one of the micrographs. The absence of carbides on coherent twin boundaries confirms previous TEM observations by Advani *et al.* [7].

These observations also provide evidence that a "critical nucleation energy" exists in which carbide precipitation occurs. This energy supplements the volume and interfacial free energy for the precipitate nucleating heterogeneously in the interface (grain boundary). It dominates at the instant of nucleation of $M_{23}C_6$ upon the boundary. It is now possible to narrow the energetic regime in which this nucleation process occurs by comparing the range of boundaries in which the specific interfacial free energy is known. The upper limit of the nucleation energy is the energy of the non-coherent twin (where precipitates were consistently observed) and the lower limit is the coherent portion of the twin (where precipitates were not at all observed). The "critical nucleation energy", $\gamma_{gb(crit.)}$, therefore, must be a value between these two boundary types ($16\ \text{mJ m}^{-2} < \gamma_{gb(crit.)} < 265\ \text{mJ m}^{-2}$ at 670 °C).

Although the evidence seems clear, one should realize that energetics alone do not dominate this system.

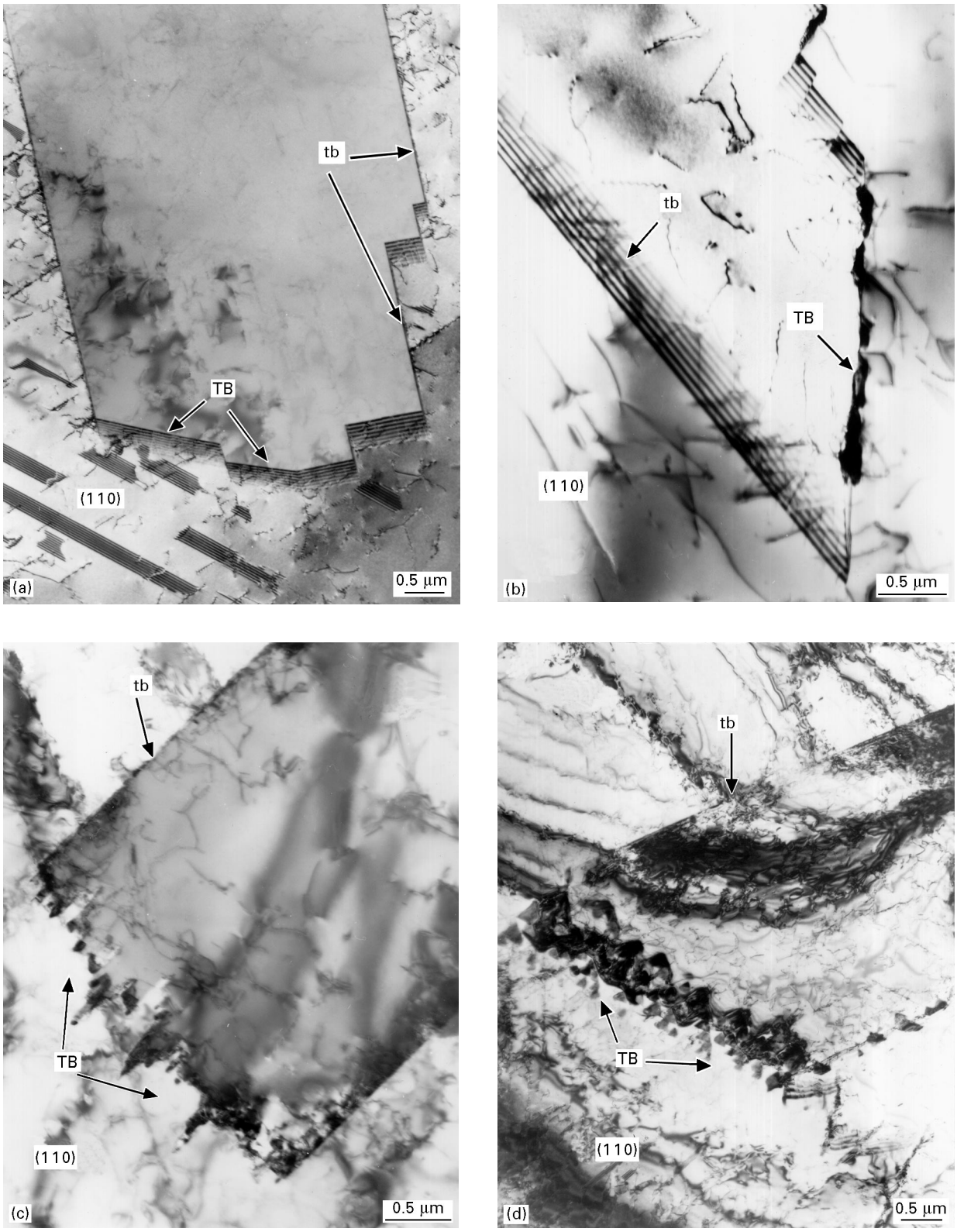


*Figure 10* TEM micrographs of the precipitation behaviour on coherent (tb) and non-coherent (TB) portions of twins in 304 stainless steel. (a) 0.01% C, (b) 0.025% C, (c) 0.05% C and (d) 0.07% C levels. While carbides are readily seen on the non-coherent twin boundaries, they were completely absent from the coherent twin boundary.

Instances where the 0.07% C material was saturated with precipitates (Fig. 6a and Fig. 10d), while the 0.01% C contained very few precipitates (Fig. 3a and Fig. 10a) is also due to the availability of carbon to diffuse and combine with chromium to form the precipitate (a thermodynamic and kinetic effect). Moreover, the thermodynamic effect may be seen by comparing non-coherent twins. All the non-coherent portions of the twins in Fig. 10a–d can generally be assumed to have the same specific interfacial free energy ($\sim 265\ mJ\ m^{-2}$). Increasing the amount of carbon on equally energetic mediums (non-coherent twins) will increase the density of precipitates that nucleate and grow on that medium.

It is now unambiguously established in this work that coherent twin boundaries do not nucleate $M_{23}C_6$ precipitates, because, as we have noted, the requisite, specific (or critical) interfacial free energy associated with this interface, is apparently too low. This means that what appears to be precipitation on coherent twin boundaries in optical metallographs, is actually precipitation on a multiplicity of steps, and appear as an etching artifact. These steps may actually form by twin boundary migration at the ageing temperatures involved, or lamellar carbides may grow extensively from such non-coherent steps in which they have nucleated, and grow parallel to, and in near coincidence with, the coherent twin boundary. Such examples of extremely long lamellar carbides have in fact been observed by Terao and Sasmal [22] and Singhal and Martin [23] and more recently by Romero and Murr [8] who discovered that this lamellar growth is also unique to specific, crystallographic twin boundaries, consistent with a resolved torque convention originally described by Murr *et al.* [24].

## 4. Conclusions

The following conclusions may be drawn from the observed data:

1. Increasing the amount of carbon in the 304 stainless steel system will result in an increase in the degree of sensitization and will increase the density of precipitates.
2. A tendency for large-angle grain boundary misorientations ($\Theta > 15^\circ$) was prevalent in all the carbon content materials and the $\{1\,1\,0\}$ grain surface orientations were found to be the major texturing direction.
3. Lower carbon steels will nucleate and grow few small sized precipitates on high-angle boundaries, while the high carbon steels will precipitate larger amounts of larger sized carbides on lower angle boundaries. The data imply that higher carbon contents need lower energies to nucleate and grow precipitates. In addition, with less than 0.07% C, carbides do not seem to fully saturate grain boundaries after 50 h at 670 °C.
4. Carbide precipitation will occur first on general grain boundaries (where the energy is the highest), then on non-coherent portions of twins (a lower energy boundary). Precipitation was not observed on coherent twins.
5. A "critical nucleation energy" must exist on a boundary for precipitation to occur. The value for this "critical nucleation energy" lies between $16\,\mathrm{mJ\,m^{-2}} < \gamma_{gb(crit.)} < 265\,\mathrm{mJ\,m^{-2}}$ which corresponds to the energies of special boundaries (non-coherent steps $265\,\mathrm{mJ\,m^{-2}}$, coherent twins: $16\,\mathrm{mJ\,m^{-2}}$; at 670 °C).


## Acknowledgements

This research was supported by the Patricia Roberts Harris Fellowship and a G. E. Faculty of the Future Fellowship (E. A. T.) and a Mr and Mrs MacIntosh Murchison Endowed Chair (L. E. M.) and in part by a U.S. DoD Defence National Stockpile Center Grant DH-009. We also gratefully acknowledge Maria Posada for her assistance in preparing samples for TEM observations.


## References


1. R. STICKLER and A. VINCKIER, *Trans. ASM* **54** (1961) 362.
2. K. T. AUST and G. PALUMBO, *Trans. Jpn Inst. Met.* **27** (1986) 995.
3. G. PALUMBO and K. T. AUST, *Acta Metall. Mater.* **38** (1990) 2343.
4. D. G. CRAWFORD and G. S. WAS, *Metall. Trans A* **23A** (1992) 1195.
5. S. SANGALL, K. J. KURZYDLOWSKI and K. TANGRI, *Acta Metall. Mater.* **39** (1991) 1281.
6. T. WATANABE, *Mater. Forum* **11** (1988) 284.
7. A. H. ADVANI, R. J. ROMERO, L. E. MURR, D. J. MATLOCK, W. W. FISHER, P. M. TARIN, C. M. CEDILLO, J. G. MALDONADO, R. C. MILLER and E. A. TRILLO, *Scripta Metall. Mater.* **27** (1992) 1759.
8. R. J. ROMERO and L. E. MURR, *Acta Metall. Mater.* **43** (1995) 461.
9. T. WATANABE, *Res. Mechanica* **11** (1984) 47.
10. J. BYSTRZYCKI, W. PRZETAKIEWICZ and K. J. KURZYDLOWSKI, *Acta Metall. Mater.* **41** (1993) 2639.
11. G. PALUMBO, K. T. AUST, U. ERB, P. J. KING, A. M. BRENNENSTUHL and P. C. LICHTENBERGER, *Phys. Stat. Solidi. (a)* **131** (1992) 425.
12. E. A. TRILLO, R. BELTRAN, J. G. MALDONADO, R. J. ROMERO, L. E. MURR, W. W. FISHER and A. H. ADVANI, *Mater. Char.* **35** (1995) 99.
13. P. LIN, G. PALUMBO, U. ERB and K. T. AUST, *Scripta Metall. Mater.* **33** (1995) 1387.
14. J. MIZERA, A. GARBACZ and K. J. KURZYDLOWSKI, *ibid.* **33** (1995) 515.
15. B. ADAMS, S. WRIGHT and K. KUNZE, *Met. Trans. A* **24A** (1993) 819.
16. L. E. MURR, "Electron and ion microscopy and microanalysis," 2nd edition (Marcel Dekker, Inc., New York, 1991).
17. R. VON MEIBOM and E. RUPP, *Z. Phys.* **82** (1933) 690.
18. B. W. BENNETT and H. W. PICKERING, *Scripta Metall. Mater.* **18** (1984) 743.
19. H. J. AARONSON, G. SPANOS, R. A. MASAMURA, R. G. VARDIMAN, D. W. MOON, E. S. K. MENON and M. G. HULL, *Mater. Sci. Engng* **B32** (1995) 107.
20. L. E. MURR, "Interfacial phenomena in metals and alloys" (Addison Wesley Publishing Co., Reading, MA 1975; reprinted by Teck Books, Fairfax, VA, 1991).
21. S. M. BRUEMMER, *Corrosion* **42** (1986) 27.
22. M. TERAO and B. SASMAL, *Metallography* **13** (1980) 117.
23. L. K. SINGHAL and J. W. MARTIN, *Acta Metall. Mater.* **15** (1967) 1603.
24. L. E. MURR, R. J. HORYLEV and W. H. LIN, *Phil. Mag.* **20** (1969) 1245.
25. L. E. MURR, G. I. WONG and R. J. HORYLEV, *Acta Metall. Mater.* **21** (1973) 595.



*Received: 27 January*
*accepted: 24 September 1997*